A SAP domain-containing protein shuttles between the nucleus and cell membranes and plays a role in adhesion and migration in *D. discoideum*

Jessica S. Kelsey and Daphne D. Blumberg*

Department of Biological Sciences, University of Maryland Baltimore County, 1000 Hilltop Circle, Baltimore, MD 21250, USA
*Author for correspondence (blumberg@umbc.edu)

Biology Open

Summary

The AmpA protein reduces cell adhesion, thereby influencing cell migration in *Dictyostelium*. To understand how *ampA* influences cell migration, second site suppressors of an AmpA overexpressing cell line were created by REMI mutagenesis. Mutant candidates were identified by their ability to suppress the large plaques that the AmpA overexpressing cells form on bacterial lawns as a result of their increased rate of migration. One suppressor gene, *sma*, encodes an uncharacterized protein, which contains a SAP DNA-binding domain and a PTEN-like domain. Using *sma* gene knockouts and Sma-mRFP expressing cell lines, a role for *sma* in influencing cell migration was uncovered. Knockouts of the *sma* gene in a wild-type background enhanced chemotaxis. An additional role for Sma in influencing cell–cell adhesion was also demonstrated. Sma protein transitions between cytosolic and nuclear localizations as a function of cell density. In growing cells migrating to folic acid it is localized to regions of actin polymerization and absent from the nucleus. A role for Sma in influencing *ampA* mRNA levels is also demonstrated. Sma additionally appears to be involved in *ampA* pathways regulating cell size, actin polymerization, and cell substrate adhesion. We present insights to the SAP domain-containing group of proteins in *Dictyostelium* and provide evidence of a role for a SAP domain-containing protein shuttling from the nucleus to sites of actin polymerization during chemotaxis to folic acid and influencing the efficiency of migration.

Introduction

Dynamic cellular movements are central in many developmental, physiological and pathological processes. An elaborate network of signaling pathways are responsible for coordinating cell movement. Through these pathways cells are able to sense environmental signals and respond directionally to those signals, a process referred to as chemotaxis. Some pathways coordinating chemotaxis are well conserved between mammalian cells and the amoeba *Dictyostelium discoideum*. Because of this conservation, *Dictyostelium* has been exploited for its use as a model system to study cell movement and chemotaxis (Parent, 2004).

Dictyostelium cell migration is important throughout its life cycle, during both its single-celled growth phase and during development where it forms multicellular fruiting bodies. During growth, cells chemotax toward folic acid produced by their food source, bacteria. In development, starved *Dictyostelium* cells move to secreted cAMP. This chemotaxis is essential in early stages of multicellular fruiting body development. A chemotactic response is initiated by the binding of a chemoattractant to cellular receptors. An intracellular amplification of the response and cellular polarization then occur, distinguishing front from rear and permitting a reorganization of the cytoskeleton. Polymerized F-actin localizes to the front of a moving cell while an actomyosin organization is present in the rear (Parent and Devreotes, 1999; Devreotes and Janetopoulos, 2003). This cytoskeletal organization allows for F-actin rich pseudopod extensions in the front and a simultaneous suppression of pseudopods and cell retraction in the rear (Parent and Devreotes, 1999; Devreotes and Janetopoulos, 2003). The well-studied PI3K signaling pathway is an example of a conserved pathway involved in chemotaxis that permits polarization of the cell and is important for cell speed and directionality (Parent, 2004). The kinase PI3K phosphorylates at the 3′ hydroxyl of phosphatidylinositol-phosphates while the lipid phosphatase, PTEN, removes this phosphate (Bagorda et al., 2006). PI3K localizes to the front of the cell and PTEN to the rear; thus at the front of the cell PI3K produces an enrichment in membrane phospholipids that allow for the binding of downstream migrational effector proteins, such as those involved in actin dynamics (Parent et al., 1998).

Another pathway shown to have roles in *Dictyostelium* migration is the *ampA* pathway (Blumberg et al., 2002; Casademunt et al., 2002; Noratel et al., 2012; Varney et al., 2002a; Varney et al., 2002b). *AmpA* mutants have been characterized revealing roles for the protein in different aspects of chemotaxis. Overexpression of AmpA protein results in an

increase in plaque size due to more rapid cell migration, and a knockout of the *ampA* gene causes a reduction in plaque size with reduced cell migration (Noratel et al., 2012). AmpA has also been shown to influence the level of actin polymerization and cellular adhesions, both important for cell migration. To try to understand the mode of action of AmpA, suppressor mutants were created that suppress the *ampAOE* increased migration phenotype. Mutants were obtained and the genes responsible for suppression were determined to have roles in chemotaxis. One of these, described here, is the *sma* gene, which encodes a protein that contains a SAP DNA-binding domain and nuclear localization signals, as well as a domain similar to phosphatase-tensin (PTEN).

The SAP domain consists of a 35 amino acid motif, which contains conserved hydrophobic and charged amino acids (Aravind and Koonin, 2000). This motif has been found in a number of chromatin associating proteins, such as scaffold attachment factors, DNA repair proteins, RNA processing complexes and proto-oncogene proteins (Ahn and Whitby, 2003; Aravind and Koonin, 2000; Böhm et al., 2005; Kipp et al., 2000). Little is known about the SAP–DNA interaction, but some evidence suggests that only a weak interaction occurs between the SAP domain and DNA. This suggests a more likely role for the SAP motif in targeting or stabilization of the DNA structural organization (Böhm et al., 2005; Kipp et al., 2000). It is also possible that the SAP domains are capable of tethering proteins involved in pre-mRNA processing to active regions of chromatin. SAP domains are found on diverse nuclear proteins and they are found in a wide range of organisms, including yeast, plants, animals, and even bacteriophage (Aravind and Koonin, 2000; Aravind and Koonin, 2001).

Disruption of *sma* in WT *Dictyostelium* cells revealed an increased efficiency in chemotaxis; but surprisingly when *sma* was disrupted in *ampAOE* cells a severe impairment in cell movement was observed. These opposing effects on chemotaxis depended on the level of AmpA mRNA in the *sma* null cells. This suggests an interaction between *sma* and *ampA* in the pathways controlling chemotaxis. In this report we characterize the novel migrational effector gene, *sma*, and present an initial characterization of its involvement in the *ampA* pathways.

Results
Identification of a novel suppressor of the *ampA* overexpression phenotype

Restriction enzyme mediated integration (REMI) mutagenesis was used to create insertional mutations in an *ampA* overexpressing (*ampAOE*) cell line. *Dictyostelium* cells grown on lawns of bacteria ingest the bacteria, migrating further into the lawn as they clear the bacteria. The clearing in the lawn is referred to as a plaque and its size reflects the ability of cells to migrate, grow, or phagocytose bacteria. The level of expression of the *ampA* gene influences the rate of migration of cells in plaques (Noratel et al., 2012). On bacterial lawns, *ampAOE* cells produce significantly larger plaque sizes than wild-type cells, and *ampA*- cells produce much smaller plaques (Fig. 1A–C,I). A suppressor of the larger *ampAOE* plaques would be expected to produce smaller plaques, likely comparable in size to wild-type or *ampA*- cell plaques. Following REMI mutagenesis more than six thousand plaques were screened for a suppression phenotype. Three mutants that produced plaques significantly reduced in size compared to *ampAOE* cells were recovered, identified, and
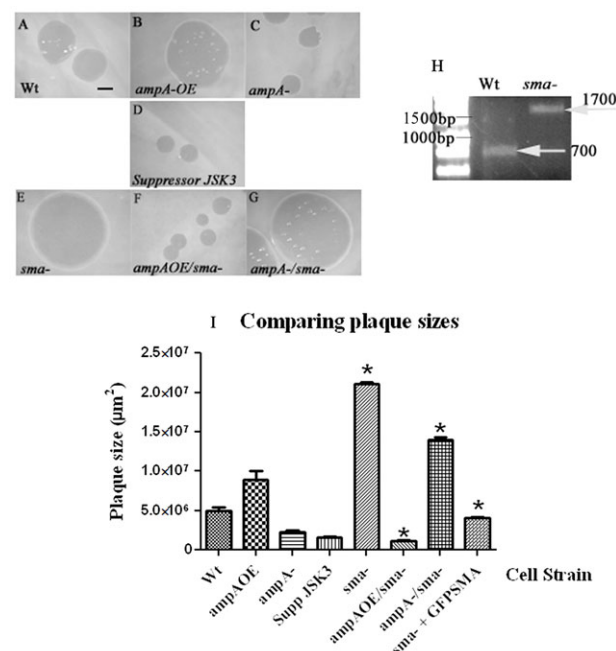

Fig. 1. The JSK3 suppressor alters plaque sizes. (A–G). WT, *ampA* and JSK3 mutant plaques formed on bacterial lawns. Scale bar: 1 mm. The areas of the plaques were determined using Metamorph (**I**). Error bars represent standard error of the mean. Plaque sizes of the rescued *sma*- cells expressing the GFP-Sma plasmid (supplementary material Fig. S3) are included in I for comparison. *Indicates a significant difference ($P<0.05$) from the parental cell type. n=a minimum of 17 plaques measured from at least 3 independent platings for each strain. (**H**) PCR results showing integration of the *sma* knockout plasmid (supplementary material Fig. S2) into the endogenous *sma* gene in the wild-type parent cells to generate the *sma*- cell line. Primers used flank the insert. WT cells produce a 700 bp fragment. *Sma*- cells produce a 1700 bp fragment.

characterized. One of these was the suppressor mutant JSK3 described here. The two other suppressor mutants have been described previously (Kelsey et al., 2012a; Kelsey et al., 2012b). Sequencing DNA flanking the REMI disruption site in JSK3 indicated that the REMI insertion resulting in the phenotypic suppression was immediately upstream of an uncharacterized gene, DDB_G0281803 (supplementary material Fig. S1). As depicted in Fig. 1D, the JSK3 suppressor mutant produced very small plaques compared to *ampAOE*. In order to determine whether it was inactivation of the adjacent DDB_G0281803 gene that was responsible for the suppression phenotype, independently generated knockouts of the adjacent DDB_G0281803 in *ampAOE* cells were created. A knockout plasmid was constructed that would remove 500 base pairs of the DDB_G0281803 gene coding region and replace them with a blasticidin resistance cassette (supplementary material Fig. S2A). This new knockout plasmid was utilized to produce DDB_G0281803 gene disruptions in *ampAOE*, wild-type and *ampA*- backgrounds. Fig. 1H shows PCR results confirming correct integration of this knockout plasmid into the WT strain to generate the knockout strain subsequently used for the characterization of the gene. Supplementary material Fig. S2B demonstrates that there is no mRNA for the DDB_G0281803 gene present in any of the 3 knockout strains generated with this plasmid (*sma*-, *ampAOE/sma*- and *ampA*-/*sma*-). The introduction of the knockout plasmid into *ampAOE* cells reproduced the significantly

decreased plaque size phenotype (Fig. 1F,I). Based on characteristics of the gene discussed below we have named it *sma* (SAP domain-containing **m**odulator of **a**dhesion).

Surprisingly, the disruption of *sma* in a wild-type or *ampA⁻* background produced an extremely large plaque phenotype (Fig. 1E,G), the opposite of what was observed when *sma* was disrupted in *ampAOE*. The plaque sizes in *sma⁻* and *ampA⁻/sma⁻* cells were more than four times the size of the original parental WT strain, making their large plaque phenotype even more pronounced than that produced by the *ampAOE* strain (Fig. 1I).

To further confirm that the phenotypes observed in *sma⁻* cells were due to a knockout of the *sma* gene, rescue plasmids were expressed in wild-type and *sma⁻* cells. A GFP-Sma rescue plasmid was constructed, which contains the full length *sma* gene with an N-terminal GFP tag (supplementary material Fig. S3). Cell lines carrying the plasmid expressed a GFP fusion protein of the correct size to be the GFP-Sma protein (~170 kDa; 144 kDa for Sma and 27 kDa for GFP). Wild-type cell lines expressing the fusion protein appeared normal; they produced plaques on bacterial lawns that were the same size as WT and they completed development normally (supplementary material Fig. S3). Introduction of the GFP-Sma plasmid into *sma⁻* cells rescued the null mutant phenotype and produced normal WT size plaques on bacterial lawns, rather than the enormous plaques seen with the *sma⁻* mutant (Fig. 1I, sma⁻+GFP-Sma), indicating that *sma* gene knockout was responsible for the altered plaque size.

Sma influences cell migration and cell–cell adhesion

Changes in plaque sizes such as those seen in *sma* knockout cells (Fig. 1) can be indicators of a defect in cell growth, phagocytosis, or cell migration. No changes in cell growth or phagocytosis were seen in *sma⁻* cells (supplementary material Fig. S4); however, significant changes in cell motility were identified in *sma* mutant cells. Migration of the different *sma* and *ampA* mutants to folic acid and to cAMP is analyzed in Fig. 2. *AmpAOE* cells produced larger plaque sizes compared to WT cells. An increase in the velocity of these cells is shown in Fig. 2A. Also, the chemotaxis plot of *ampAOE* cells reveals longer path lengths (Fig. 2B). This confirms our previous observation that the increased velocity in *ampAOE* cells permits an increase in plaque size compared to WT (Noratel et al., 2012). *Sma⁻* cells also produced significantly larger plaques compared to WT. As indicated in Fig. 2A, *sma⁻* cells moved faster, were significantly more directional, and displayed an increased chemotactic index (Fig. 2A). This is also evident in the chemotaxis plots in Fig. 2B. Together, these chemotaxis effects permit a quicker, more directional movement to the chemoattractant, which could explain the increased plaque sizes in *sma⁻* cells. As expected based on plaque sizes, *ampA⁻/sma⁻* cells also display an increased efficiency in chemotaxis compared to WT cells (Fig. 2A). Unlike the *ampA⁻* cells, which show a decreased rate of migration (Noratel et al., 2012), the *ampA⁻/sma⁻* cells show the same velocity as WT cells but they show greater directionality and chemotactic index. The *sma⁻* defect in chemotaxis appears to be specific for chemotaxis to
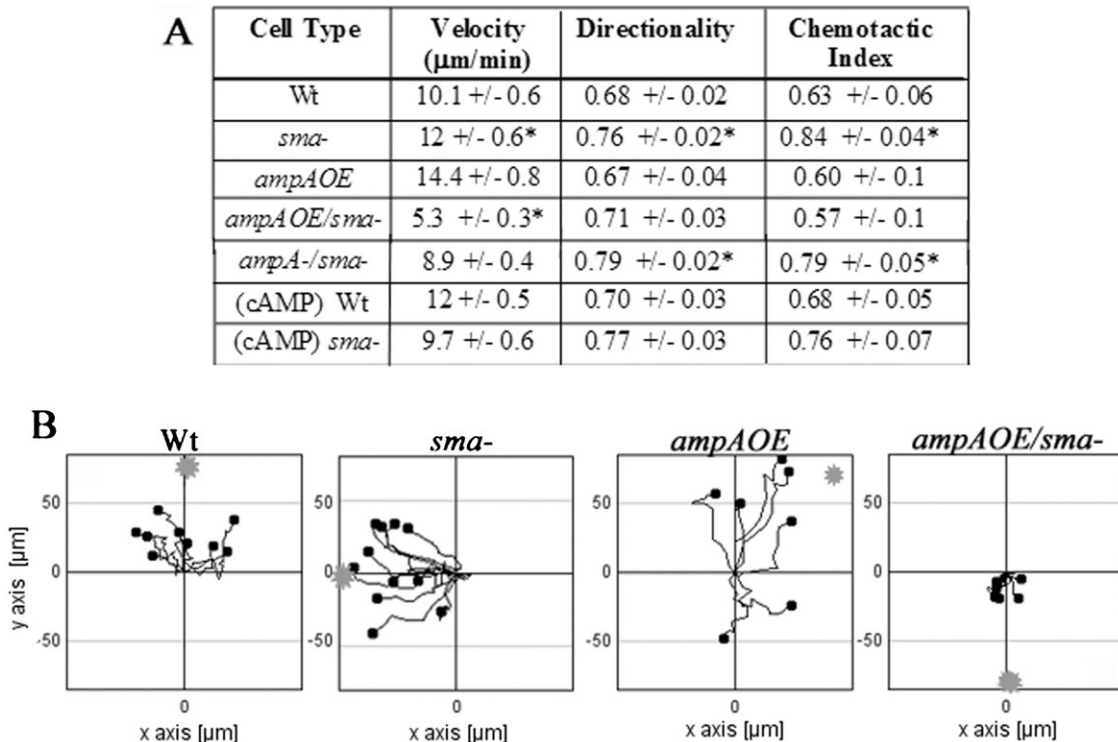
A

Cell Type	Velocity (µm/min)	Directionality	Chemotactic Index
Wt	10.1 +/- 0.6	0.68 +/- 0.02	0.63 +/- 0.06
sma-	12 +/- 0.6*	0.76 +/- 0.02*	0.84 +/- 0.04*
ampAOE	14.4 +/- 0.8	0.67 +/- 0.04	0.60 +/- 0.1
ampAOE/sma-	5.3 +/- 0.3*	0.71 +/- 0.03	0.57 +/- 0.1
ampA-/sma-	8.9 +/- 0.4	0.79 +/- 0.02*	0.79 +/- 0.05*
(cAMP) Wt	12 +/- 0.5	0.70 +/- 0.03	0.68 +/- 0.05
(cAMP) *sma-*	9.7 +/- 0.6	0.77 +/- 0.03	0.76 +/- 0.07

Fig. 2. The role of *sma* in cell migration. Chemotaxis of growing cells towards folic acid was analyzed. (**A**) Values of velocity (µm/min), directionality, and the chemotactic index for the indicated cell types. Cells were tracked on agar with images acquired every 20 seconds for 5 minutes. A minimum of at least 20 cells for each strain was tracked in 3 different rounds of chemotaxis on different days. *Indicates a significant difference of *sma⁻* strains compared to WT or *ampA*OE parental strains with $P<0.05$ using a Student's *t*-test. Chemotaxis to cAMP was measured using 6-hour developing cells. (**B**) Chemotaxis plots from representative fields. The direction and distance of each cell from its origin at $t=0$ is shown. The location of the source of chemoattractant is indicated in each plot by a gray star.

folic acid, as rates and directionality of chemotaxis to cAMP in *sma*⁻ cells were not significantly changed (Fig. 2A).

By contrast to the situation in WT cells, overexpression of AmpA protein in *sma*⁻ cells (*ampAOE/sma*⁻) caused formation of small plaques. Consistent with this, *ampAOE/sma*⁻ cells displayed a significantly decreased rate of migration (Fig. 2A). This defect is clearly illustrated in the chemotaxis plots where *ampAOE/sma*⁻ cells are shown moving very little from the origin (Fig. 2B).

The *sma* gene also appears to play a role in cell–cell adhesion. As depicted in Fig. 3A, *sma* knockout cells tended to clump more during vegetative growth than WT cells. The graph in Fig. 3B gives values for the percent of cells found in clumps of three or more. While only about 10% of wild-type cells were found in clumps, over 30% of *sma*⁻ cells were found in clumps.

The effects of the *sma* gene knockout on cell migration and cell–cell adhesions provide evidence of a role for *sma* in two pathways known to be influenced by the *ampA* gene (Noratel et al., 2012; Varney et al., 2002a). The results also suggest a complex interaction between *ampA* and *sma*. Below, we further characterize the *sma* gene in WT cells. The *ampA/sma* interaction is also investigated and discussed later.

DDB_G0281803 or *sma* contains protein domains suggesting possible functions

The *sma* gene encodes a 1216 amino acid, 144 kDa protein, with no known homologs identifiable from BLAST searches. A
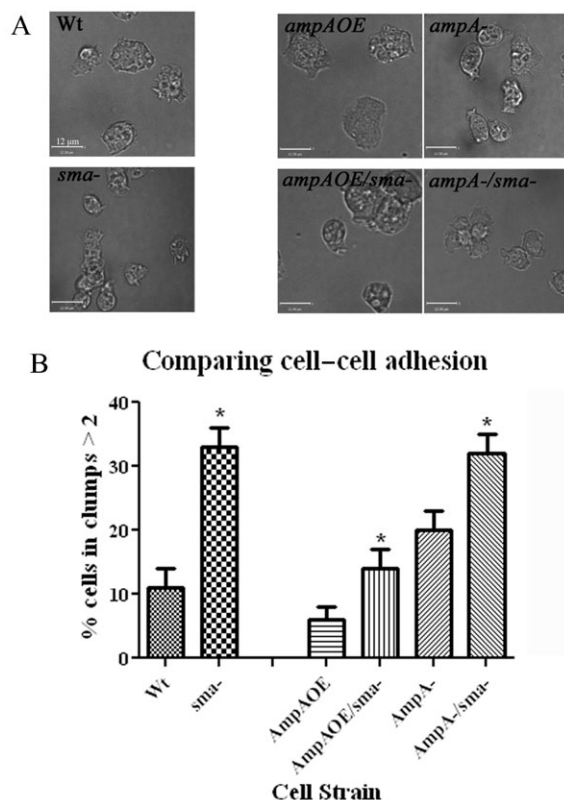
number of putative protein domains were detected using Motif Scan (Pagni et al., 2007). These include a G-binding formin 3-homology domain (GBD-FH3), a phosphatase tensin domain (PTEN), a SAP DNA-binding domain (SAP), and two nuclear localization signals (NLS) (Fig. 4A). G-binding formin 3 homology domains are N-terminal domains found in some formins (Rivero and Somesh, 2002). Formins are actin-binding proteins that promote the formation of linear actin filaments. The FH3 domain of formins is thought to be important for targeting the proteins (Rivero et al., 2005). A G-binding domain is present in the FH3 domain where interactions with Rho GTPases have been described. Rho-GTPases are essential in a number of actin dynamic processes (Rivero and Somesh, 2002). Phosphatase tensin domains are known to be involved in signaling pathways regulating actin polymerization and cell migration (Leslie et al., 2005). PTEN (phosphatase tensin homolog deleted on chromosome 10) is probably the most well-known protein in that family. In *Dictyostelium* it acts as an inhibitor of the PI3K signaling pathway that permits polarization and regulates cell migration and directionality (Leslie et al., 2005).

The SAP domain is a DNA-binding motif named after the proteins in which it was originally identified: **S**AF-A/B, **A**cinus and **P**IAS (Aravind and Koonin, 2000). Alignment of the Sma SAP domain with other SAP domains from mammalian and yeast proteins indicates that Sma contains the same key features of this domain including the two stretches of conserved hydrophobic amino acids separated by a region that includes a conserved glycine (Fig. 4B) (Aravind and Koonin, 2000). Sma also is predicted to have the conserved alpha helices in the two hydrophobic regions found in all SAP domains (Aravind and Koonin, 2000). These hallmark helical regions, along with the conserved positively charged amino acids, are proposed to make contact with DNA (Aravind and Koonin, 2000; Aravind and
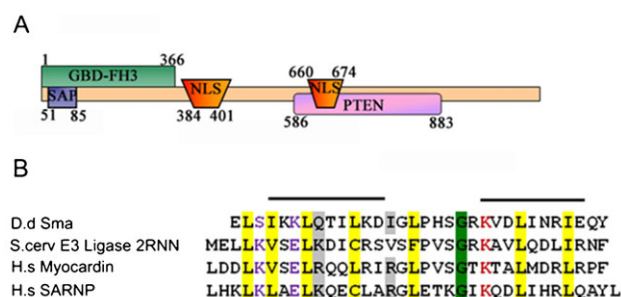

Fig. 3. Sma affects cell–cell adhesions. (**A**) Images of exponentially growing cells. Scale bars: 12 μm. (**B**) Percent of cells found in clumps of more than 2 cells. Error bars represent standard error of the mean. *Represents a significant difference from the parental strain with *P*<0.05 using a Student's *t*-test. *n*=at least 3 independent experiments done with different batches of cells grown on different days.

Fig. 4. The predicted protein domains in *sma*. (**A**) Predicted protein domains in the *sma* suppressor gene determined using Motif Scan (Pagni et al., 2007) are shown with amino acid positions listed next to each. The regions are: SAP for SAP DNA-binding domain, GBD-FH3 for G-protein-binding formin homology 3, PTEN for phosphatase tensin domain, and NLS for nuclear localization signal. (**B**) ClustalW2 alignment of the predicted SAP domain from Sma with SAP domain sequences from *H. sapiens* (Myocardin accession no. AAV33439, and SARNP accession no. NP_149073.1) and from *S. cerevisiae* (an E3 ligase, accession no. 2RNN). Characteristics of the SAP domains are colored as described previously (Aravind and Koonin, 2000) and represent a 90% consensus among the initial SAP domains that they identified: hydrophobic or aliphatic residues (YFWLIVMAC) are in yellow, polar residues (STQNEDRKH) are in purple, bulky residues (KREQWFYLMI) are in gray, an absolutely conserved glycine (G) is green and a highly conserved lysine (K) is red. Two amphipathic helices were determined for the Sma protein using the PredictProtein program and are overlined. They match perfectly with the positions of the amphipathic helices in the SAP domain alignment characterized previously (Aravind and Koonin, 2000).

Koonin, 2001). Like the Sma protein described here, most proteins carrying a SAP domain are multi-domain proteins. Interestingly, SAP domain-containing proteins are present in all Dictyostelia subgroups. *Dictyostelium discoideum* has about 20 SAP domain-containing proteins, none of which have been characterized (Gaudet et al., 2011; Gaudet et al., 2008). The different domains present in each of the 20 SAP domain-containing proteins in *Dictyostelium discoideum* appear unique for each protein, with few similarities among them (supplementary material Fig. S5). It appears the SAP domain is not specific to the N-terminus, where it is in Sma. Also, no other SAP domain-containing protein contains exactly the same additional domains as found in Sma. There is one that also contains a PTEN domain and another that contains a cortactin domain, raising the possibility that other SAP domain-containing proteins in *Dictyostelium* may also interact with the cytoskeleton (supplementary material Fig. S5). This represents a departure for SAP domain-containing proteins, as most are associated with proteins domains involved in DNA repair, RNA processing, or that suggest a function as chromatin scaffold proteins.

A predicted SAP domain suggests an interaction with DNA. This is in agreement with the presence of two predicted nuclear localization signals found in Sma.

Sma protein is localized in part to the nucleus, but at high cell densities an increasing amount is found in the membrane fraction during growth

In order to localize the Sma protein in cells a portion of the *sma* gene coding region was fused to an mRFPmars protein and used to generate a gene replacement strain in which the Sma-mRFP protein is expressed under the control of the endogenous *sma* promoter. Expression of the fusion protein under its own control regions should mimic the normal expression of the Sma-protein. The Sma-mRFP expressing cells were demonstrated to have the wild-type gene replaced with the Sma-mRFP fusion gene and were shown to express the correct size protein product (supplementary material Fig. S6). The Sma-mRFP gene replacement strain retained the WT phenotype both with regard to plaque size and developmental progression indicating that the Sma-mRFP gene is functional (supplementary material Fig. S6). It was necessary to use indirect immunofluorescence microscopy with fixed cells to detect the mRFP fusion protein in *Dictyostelium* cells because the *sma* gene is expressed at a sufficiently low level that the amount of Sma-mRFP fusion protein produced resulted in fluorescence too weak to detect with laser power that did not kill the cells.

Sma protein levels increased as a function of cell density in vegetative cells. The protein appeared localized to the nucleus but at high densities increasing amounts of the protein localized to the cell periphery (Fig. 5). Fig. 5A,B reveal an increase in the fluorescent intensity of the Sma-mRFP signal as cells progressed from low to high density. An increase in Sma-mRFP protein product with increasing cell densities was also seen in western blots (Fig. 5C) confirming the expression trend seen by immunofluorescence (Fig. 5A,B).

Interestingly, the GFP-Sma fusion protein, which was expressed under the control of the high level actin promoter and introduced into cells on a high copy number plasmid, was detected mostly near the nucleus (supplementary material Fig. S3). The overexpressed GFP-Sma, even at high density, seemed to remain mostly nuclear although a small amount of GFP-Sma
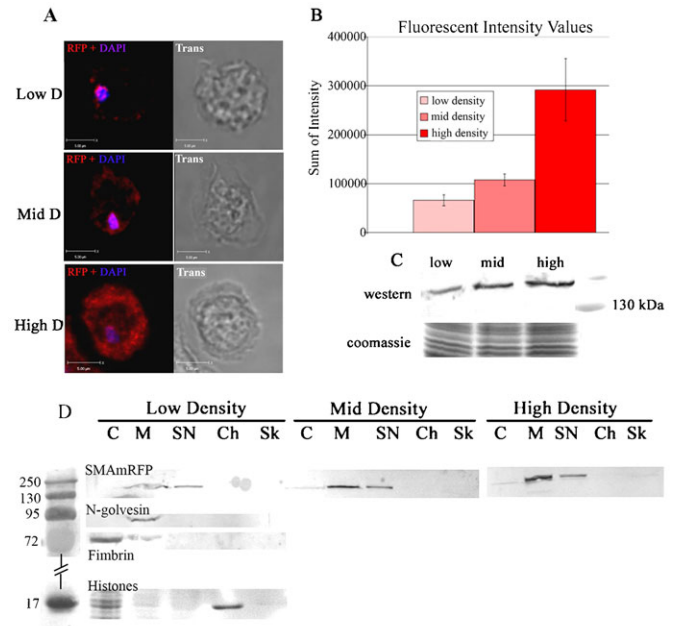

Fig. 5. Sma expression and localization during growth. (A) Sma-mRFP expressing cells at different cell densities were fixed and stained with anti-RFP antibody (red). The nucleus is stained with DAPI (blue). Images are Z-axis slices through the cells. Scale bars: 5 μm. Low-density cells ($<1\times10^6$ cells/ml); mid-density cells (2–4×10^6 cells/ml); high-density cells ($>6\times10^6$ cells/ml). **(B)** Fluorescent intensity at increasing cell densities. Error bars represent standard error of the mean. Fluorescence intensity from individual optical sections of the entire confocal volume of at least 15 cells was summed and averaged per cell for each density. The Y-axis is the average sum of fluorescent intensity per cell. **(C)** Western blot of Sma-mRFP protein levels at different densities (top); Coomassie staining (bottom). The Sma-mRFP protein was detected by anti-RFP antibody. **(D)** Cell fractionation at low, mid, and high densities. C – cytoplasm, M – membrane, SN – soluble nuclear, Ch – chromatin bound, Sk – cytoskeletal. Western blot (top) with anti-RFP antibody to detect Sma protein; bottom 3 panels show controls. To detect golgi and golgi derived vesicle location, GFP-N-golvesin (91 kDa) and a GFP antibody were used. Localization of the soluble actin-binding protein fimbrin is shown (fimbrin antibody, 67 kDa). Coomassie staining showed histone localization to the chromatin fraction (~17 kDa).

was seen at the cell periphery. This is in contrast to the increased distribution of Sma at the cell periphery in the Sma-mRFP knockin construct, which was expressed under the control of the endogenous *sma* promoter that is a much lower level promoter and is present at only 1 copy per cell. This suggests the nucleus may be the default localization for Sma. Possibly it requires an interaction partner that is limiting to transport it to the cell periphery.

Sma-mRFP cells at increasing densities were fractionated, and Sma-mRFP was predominantly in membrane fractions and in the soluble nuclear fraction (Fig. 5D). Interestingly, the amount of Sma in the soluble nuclear fraction remained fairly constant, while the amount in the membrane fraction increased with increasing cell density.

Sma protein leaves the nucleus and localizes to the ends of cells during migration to folic acid but remains in its nuclear location when starving cells migrate to cAMP

Because Sma clearly plays a role in cell migration it was of interest to determine whether it showed any interaction with the actin cytoskeleton and whether its localization changed in

migrating cells. As expected based on the fractionation results shown in Fig. 5, a positive correlation of Sma-mRFP localization with the DAPI stained nucleus was found in vegetatively-growing cells (Fig. 5, Fig. 6D for the Pearson's coefficient). A small but positive correlation between Sma-mRFP and F-actin was also determined (Fig. 6A,D). There are small patches where there is colocalization between Sma and F-actin (yellow arrow in Fig. 6A). A perfect colocalization would give a Pearson's coefficient value of 1.0. The values for nuclear (0.35) and F-actin (0.08) colocalization with Sma-mRFP during vegetative growth in medium-density cells were much lower, suggesting only some of the Sma-mRFP localized with these organelles/
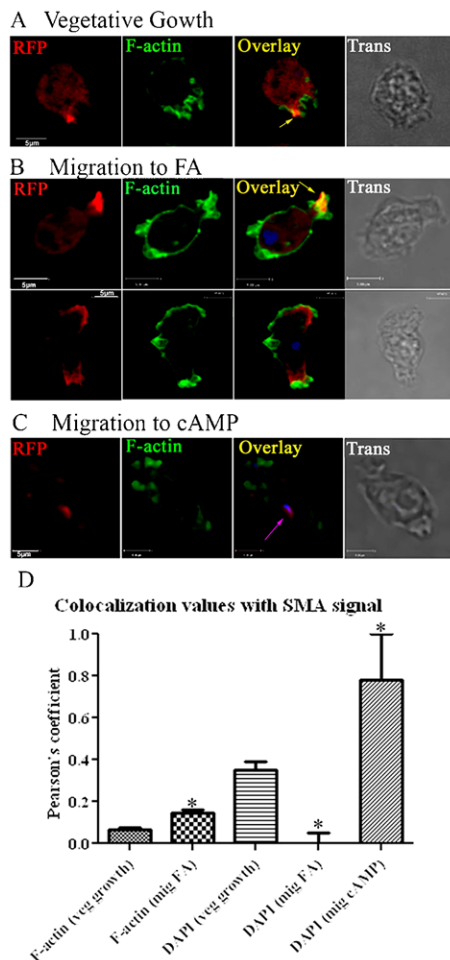

Fig. 6. Localization of Sma during growth and migration. Cells were fixed and labeled for Sma-mRFP (anti-RFP antibody, red), nuclei (DAPI, blue), and F-actin (phalloidin, green). The overlay depicts areas of colocalization between signals (yellow or pink). (**A**) Medium-density vegetatively-growing cells. (**B**) Cells in growth phase migrating to folic acid. (**C**) Starved cells migrating to cAMP. Images are Z-axis slices through cells. Scale bars: 5 μm. (**D**) Pearson's coefficient values for Sma-mRFP and F-actin in growing and migrating cells (first 2 columns). Also shown are the values for Sma-mRFP and DAPI during growth, migration to folic acid, and during migration to cAMP (last 3 columns). The control was the value of F-actin and DAPI correlation, which would represent zero colocalization. While the images shown are single optical sections, the Pearson's coefficient is calculated over the entire Z stack and represents the X, Y and Z probability of colocalization. $n=15+$ cells, from at least 3 independent rounds of staining. *Indicates a significant difference with $P<0.05$ using a Student's t-test.

proteins. The remainder of the Sma protein would appear to be in the cellular membrane fractions (Fig. 5D).

Fig. 6B shows images of elongated cells migrating to folic acid. Sma-mRFP and polymerized F-actin are labeled. Upon migration to folic acid much of the Sma protein was seen concentrated to the poles of the moving vegetative cells and it appeared to completely leave the nucleus. In some cells a small portion of the Sma protein was seen concentrated in F-actin rich extensions (Fig. 6B, top). In other cells Sma appears polarized and localized to regions adjacent to F-actin (Fig. 6B, bottom). Fig. 6D reveals a colocalization value for Sma and F-actin of 0.13. This value is low and reflects the fact that Sma is mostly seen localized just outside regions of actin polymerization. In migrating cells chemotaxing to folic acid, Sma appeared to be totally absent from the nucleus (Fig. 6B,D). The colocalization values in Fig. 6D show a Pearson's coefficient of zero for the Sma-mRFP signal and the DAPI signal in folic acid chemotaxing cells indicating complete absence from the nucleus. The same increased localization of Sma to the poles of cells migrating to folic acid was observed using the actin promoter driven GFP-Sma fusion construct (supplementary material Fig. S3E, bottom). The excess GFP-Sma fusion protein expressed under the control of the actin promoter remains in association with the nucleus, in contrast to the complete loss of Sma protein from the nucleus when the endogenous *sma* promoter, which is a much lower level promoter, is used to drive expression of the fusion protein.

When cells were starved for development for 6 hours and migrating to cAMP, a very different result was observed. The Sma-mRFP protein remained almost entirely associated with the nucleus. The amount of colocalization between Sma-mRFP and DAPI was significantly increased showing a Pearson's coefficient of 0.8, reflecting almost complete localization to the nucleus (Fig. 6D). Fig. 6C shows the almost complete nuclear localization of Sma-mRFP in starved cells migrating to cAMP although a small amount of the Sma is present in the cytoplasmic membranes but not at the poles of cells. Thus, in growing cells migrating to folic acid Sma leaves the nucleus and a portion of it becomes polarized to the ends of the cell with some Sma found associated with the F-actin cytoskeleton. By contrast, in starving cells migrating to cAMP, Sma largely remained in the nucleus.

Sma functions in the *ampA* pathway

A disruption in *sma* caused suppression in the *ampAOE* pathway controlling plaque sizes. This was evident in the considerably smaller plaques produced by *ampAOE/sma*^{−} cells, compared to *ampAOE* cells (Fig. 1). Sma has a SAP DNA-binding domain suggesting the possibility of gene regulation or RNA interactions. Could Sma regulate *ampA* expression? To determine if a disruption in *sma* interferes with AmpA mRNA accumulation, transcript levels of *ampA* were monitored when *sma* was disrupted. The results (Fig. 7A) show a decrease in *ampA* mRNA transcripts when *sma* was disrupted. When Sma was knocked out, the level of *ampA* transcripts in *ampAOE* cells decreased to near WT levels, and WT *ampA* transcript levels appeared to decrease even further in the *sma*^{−} cells. It appears that Sma is necessary for full levels of *ampA* mRNA accumulation, and in *sma*^{−} cells an almost compete loss in *ampA* transcript is observed.

The RT-PCR results shown in Fig. 7A suggest that a Sma knockout is equivalent to an AmpA knockout with respect to *ampA* mRNA levels, so we investigated the effect of *sma*
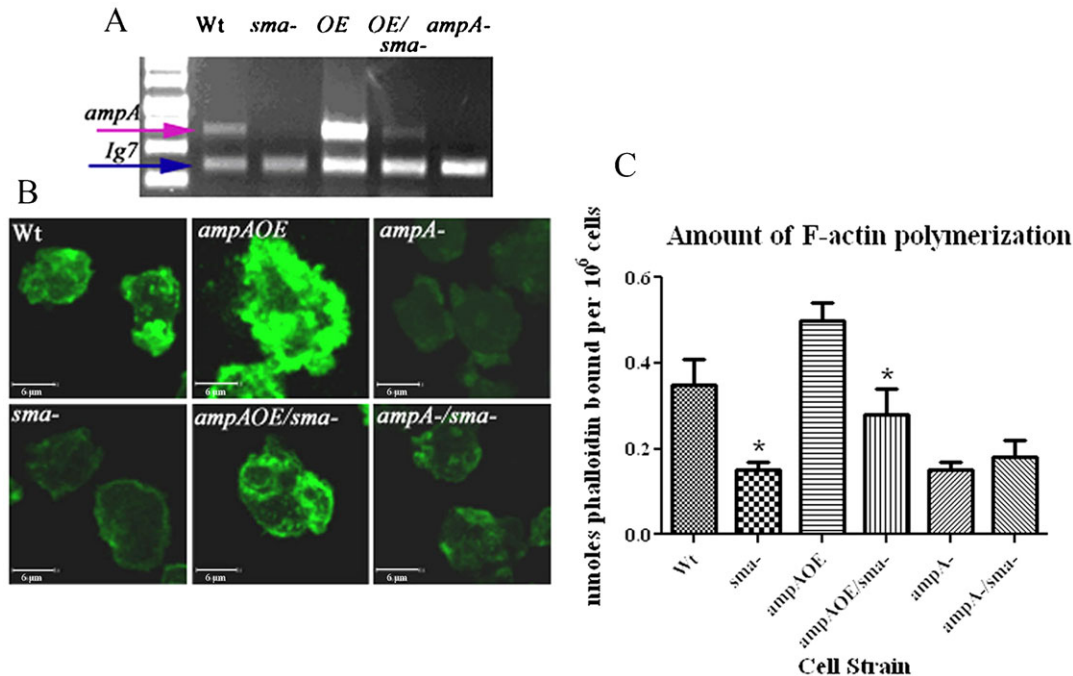
Fig. 7. The *sma* gene is necessary for *ampA* mRNA accumulation and its loss phenocopies some *ampA* effects. (A) RT-PCR showing levels of *ampA* transcripts in *sma* knockout and *amp*A mutant cell lines. The higher band represents the *ampA* transcript product of 700 bp. The lower band is the 370 bp Ig7 control product. Similar results were obtained on at least 3 different repeats on different days with different mRNA preparations. (**B**) *Sma* knockout cells in the different *ampA* parental strains were fixed and stained with Alexa-488 phalloidin (green) to visualize F-actin. Images are 3D reconstructions from a confocal Z series. Scale bars: 6 µm. (**C**) The level of actin polymerization was measured by quantifying the amount of alexa-488-phalloidin binding to cell extracts. *Indicates a significant difference from the parental strain with $P<0.05$ using a Student's *t*-test. $n=$at least 2 rounds of measurements on cells grown on different days.

disruption on the different *ampA* pathways to try to confirm this relationship. The phenotypic differences of *ampA⁻* or *ampAOE* cells compared to WT are shown in Figs 7 and 8. *AmpA⁻* cells polymerize less actin compared to WT cells, are smaller in size, and display increased cell–substrate adhesion. The opposite is true for *ampAOE* cells, which produce increased levels of actin polymerization, show larger cell sizes, and decreased cell–substrate adhesions. Based on the RT-PCR results, we would expect to see *sma⁻* phenotypes similar to *ampA⁻* and *ampAOE*/*sma⁻* phenotypes similar to WT. As indicated below, this does appear to be the case. Fig. 7B shows images of alexa fluor 488-phalloidin staining of polymerized F-actin in vegetative cells. A

disruption of *sma* in wild-type and *ampAOE* cells resulted in a decrease in the amount of F-actin. There was no further decrease in actin in *ampA⁻/sma⁻*. The bar graph in Fig. 7C shows the amount of alexa-fluor 488-phalloidin binding to F-actin in the different cell types. The decrease in the amount of F-actin when *sma* was disrupted in WT was equivalent to levels seen in *ampA⁻* cells, WT cells had 2× more F-actin than did *sma⁻* and *ampA⁻* cells. Also, the amount of polymerized actin in *ampAOE/sma⁻* cells was near WT levels, *ampAOE* cells contained 1.5× the amount of polymerized actin found in WT and *ampAOE/sma⁻* cells. The same trend was found in the cell size and cell–substrate adhesion assays. The bar graph in Fig. 8A shows a significant
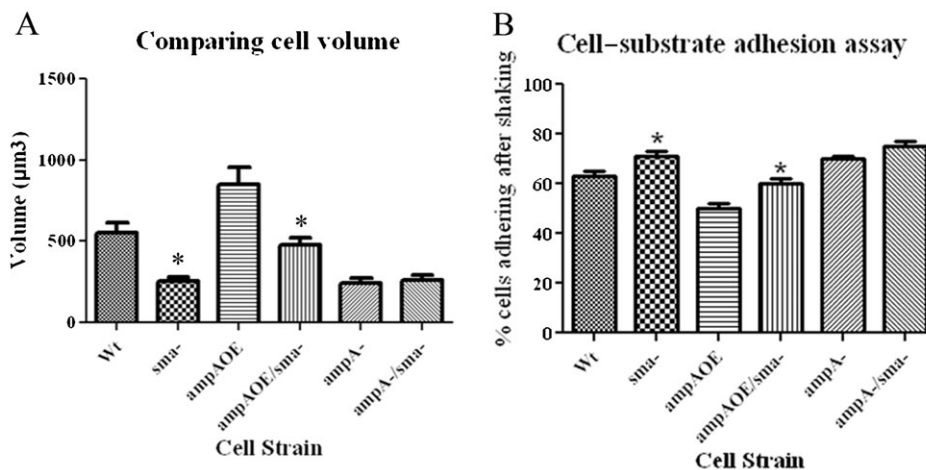

Fig. 8. *Sma* has a role in *ampA* pathways controlling cell size and substrate adhesion. (**A**) Cell volume (µm³) during growth was measured using the volume measurement function of Velocity with 3D reconstructions of Z series using G-actin (DNase I) stained cells. Error bars represent standard error of the mean. At least 20 cells were measured per strain in 3 independent experiments on different days. (**B**) Cell–substrate adhesion indicated by the percent of the cells remaining attached to the substrate after 45 minutes at a shaker speed of 50 rotations per minute (RPM). Error bars represent standard error of the mean. *Indicates a significant difference from the parental strain, with $P<0.05$ using a Student's *t*-test. $n=3$ rounds of measurements on different days.

decrease in cell volumes when the *sma* gene was disrupted in WT and *ampA*OE cells. The differences in cell sizes can be viewed in the images in Fig. 3A. The cell volume of *ampA⁻* cells was similar to the cell volume of *sma⁻* cells and there was no further decrease in cell volume in the *ampA⁻/sma⁻* double mutant suggesting that the loss/decrease in *ampA* mRNA in the *sma⁻* cells was sufficient to account for the decrease in cell volume. Likewise, the knockout of *sma* in the *ampA*OE strain reduced the enlarged volume of the *ampA*OE cells to close to the volume of WT cells.

To compare cell–substrate adhesion, the percentage of adhesive cells that remained attached to Petri dishes after shaking was determined (Fig. 8B). A significant increase in cell–substrate adhesion was seen in *sma⁻* cells compared to WT and in *ampA*OE/*sma⁻* cells compared to *ampA*OE. In *ampA*OE/*sma⁻* 60% of the cells were highly adhesive, similar to the WT level of 63%. *Sma⁻* cells displayed 71% of their cells as highly adhesive, very similar to the *ampA⁻* level of 70%. The assays in Figs 7 and 8 display a clear trend where the disruption of *sma* causes a change in *ampA*OE phenotypes to WT, and a disruption of *sma* in WT cells mimics or phenocopies the *ampA⁻* phenotype. A *sma* disruption in *ampA⁻* cells appeared to have no additive effect on the assays shown in Figs 7 and 8. A double knockout of genes in different pathways usually results in an additive effect, which should produce phenotypes more severe than either mutant alone. The phenotypes of the double knockout mutant, *ampA⁻/sma⁻*, were not significantly different than either mutant alone, suggesting that *sma* and *ampA* are involved in the same pathway controlling actin polymerization, cell size, and substrate adhesion. Potentially the *sma* gene acts upstream of *ampA* controlling its level of mRNA accumulation.

The role of Sma in cell–cell adhesion exceeds its role in *ampA* expression

Both *ampA* and *sma* knockouts resulted in increases in cell–cell adhesion as assayed by counting cells in clumps of 3 or more (Fig. 3A,B). However, the effect of *sma* on cell–cell adhesion was much stronger than the effect of *ampA*. *Sma* null cells showed over 30% of growing cells in clumps ($3\times$ the wild-type level) while *ampA* null cells showed only 20% or twice the wild-type level of cell clumping ($P<0.05$) (Fig. 3B). Overexpression of *ampA* resulted in reduced cell–cell clumping to about half of the wild-type levels (Fig. 3B). The loss of *sma* in the *ampA* overexpressing strain (*ampA*OE/*sma⁻*) increased clumping to 1.5 times the wild-type level. The *sma⁻/ampA⁻* double mutant showed the same higher level of clumping that *sma⁻* alone shows. This is in contrast to the results with actin polymerization, cell volume and cell–substrate adhesion where the level of effect of the *sma* null mutation is identical to the effect of the *ampA* null mutation alone, suggesting that the role of *sma* is confined to its effects on *ampA* mRNA levels for these events. For cell–cell adhesion by contrast *sma* has a role in addition to being necessary for *ampA* mRNA accumulation.

Sma is necessary for development

Sma expression increased during development, with a peak level at about 12 hours (supplementary material Fig. S7). Disruption of *sma* also resulted in the inability of cells to produce the later fruiting body structures (supplementary material Fig. S8). Interestingly, the developmental defect in the *sma⁻* cells was more severe than the defect in *ampA⁻* cells. AmpA null cells

showed a 6-hour delay in development but eventually formed fruiting bodies (Varney et al., 2002b). By contrast, the *sma⁻* cells formed rough flattened mounds with only an occasional fruiting body. This is consistent with the fact that while *sma* may regulate *ampA*, it also appears to have additional functions. Sma-mRFP expressing cells are distributed throughout the early finger structures where a faintly dispersed signal was seen (supplementary material Fig. S8). This suggests Sma is not restricted to a specific cell type during development. This also differs from *ampA* because *ampA* expression during development is confined to the Anterior-Like Cells.

Discussion

We have characterized a gene involved in a signaling pathway important for chemotaxis. An interaction between the newly identified *sma* pathway and the *ampA* pathway in influencing chemotaxis is demonstrated. *Sma* appears to have a role in cell migration, as mutants with disruptions in the *sma* gene are more efficient in chemotaxis. Interestingly, the presence of AmpA strongly interferes with the more efficient *sma⁻* mutant strain's chemotaxis and impairs cell movement. This is in contrast to the fact that overexpressing AmpA in *sma⁺* wild-type cells increases cell migration. We have presented an initial characterization of the *sma* gene and of its unexpected interaction with *ampA*.

Sma expression in the cell

Sma protein levels increased as the density of growing cells increased. A low level of Sma localization to the nucleus appeared consistently throughout the growing cell densities using both cell fractionation techniques and immunofluorescence microscopy. As cells reached higher densities an increasing amount of the Sma protein localized to the cytoplasmic membrane fractions, especially at the cell periphery. Consistent with this location at the cell periphery at high cell densities, a knockout of Sma resulted in severe clumping of the cells indicating a role for Sma in reducing cell–cell adhesions. Together these results point to a possible role in regulating cell–cell adhesions in a density-dependent manner.

The predicted SAP DNA-binding domain and nuclear localization signals in the Sma protein, as well as the fact that some of the Sma protein is localized to the nucleus, suggests a role for Sma in DNA binding, chromatin interaction, or some aspect of gene expression. Indeed, Sma plays a role in regulating *ampA* mRNA levels. The fact that Sma is present in the soluble nuclear fraction and not in the chromatin fraction, however, suggests that Sma has only an indirect role in DNA binding or transcription. Alternatively it could play a role in RNA processing, transport out of the nucleus or RNA stability. The *ampA* gene does not have any introns so any controls at the level of RNA processing are not likely to involve RNA splicing. Further investigation is required to fully understand the role of Sma in controling *ampA* mRNA levels. Interestingly, however, the default location of Sma appears to be the nucleus because when the Sma protein is overexpressed from an actin promoter on a high copy number plasmid the extra Sma protein localizes to the nucleus and in fact the very intense nuclear staining in the overexpressing Sma strains almost obscures the Sma that is localized to the cytoplasmic membranes at the cell periphery. This raises the possibility that a factor whose concentration is limiting is required for Sma to exit the nucleus and localize to the cytoplasmic membrane fraction.

A role for Sma in chemotaxis

In migrating cells chemotaxing to folic acid Sma appears to completely leave the nucleus and translocate to the poles of the cells and to localize immediately adjacent to F-actin rich regions with some Sma actually colocalizing with F-actin. This could imply a role for Sma in actin dynamic processes. Supporting this role was the predicted GBD-FH3 domain, a domain involved in G-protein interactions regulating actin dynamics (Rivero et al., 2005; Rivero and Somesh, 2002). The possibility of a SAP domain-containing protein interacting with actin is not completely novel. The SAP domain-containing transcription factor MKL (myocardin-like protein) was found to change its subcellular localization as a function of the Rho-actin signaling pathway (Du et al., 2004; Miralles et al., 2003). Rho signaling promoting actin polymerization resulted in a shift of MKL localization, from the nucleus to the cytoplasm, where it was seen colocalizing with actin. It is possible that a similar signaling event recruits Sma to the cytoplasm, to regions adjacent to actin polymerization.

Another putative domain in Sma, the PTEN-like domain, is important in the regulation of signaling pathways contributing to cell polarization in migrating cells (Leslie et al., 2005). Sma^- cells appear to be very efficient in chemotaxis, more so than wild-type cells. It is the chemotactic index that is particularly increased in the sma gene knockout. Sma localization in folic acid migrating cells was predominately at the cell poles. This raises the question of a possible role for Sma in the cell polarization process. The Sma presence at the poles of the cell could help regulate specific signaling pathways during chemotaxis. A key question is how the absence of Sma results in a cell more effective in chemotaxis.

Sma was mostly absent from the nuclear region in cells chemotaxing to folic acid but remained in the nucleus in starved cells migrating to cAMP. In fact, in starved cells migrating to cAMP, almost no Sma was detected in the cytoplasm. Also, the sma^- increased migration defect was detected only in cells chemotaxing to folic acid and not in those chemotaxing to cAMP. This suggests a role for Sma in migration only during the vegetative-growth phase, when cells migrate in search of bacteria, which they locate via folic acid.

Comparison of folate chemotaxis with cAMP chemotaxis indicates that four pathways essential for signal amplification during chemotaxis to cAMP are activated by folate but do not appear to be essential for chemotaxis to it (Kortholt et al., 2011). As a result the chemotactic response to folate requires a steeper gradient and shows a reduced chemotactic index compared to cells migrating up a steep optimal cAMP gradient (Kortholt et al., 2011). It has also been suggested that because of the need to frequently change direction in the search for bacteria, growing cells remain sensitive to chemoattractants across their entire periphery, which would result in reduced polarization and a reduced chemotactic index relative to cells migrating very directionally to a cAMP source (Janetopoulos and Firtel, 2008). Sma clearly plays a role in reducing the chemotactic index in growing cells but how it does this or if it might interact with any of the 4 pathways that function to amplify the chemotactic signal is clearly an issue for the future.

Sma and AmpA

Sma appears to control the level of ampA mRNA accumulation. While the effect of sma knockouts on cell size, cell–substrate

adhesion and actin polymerization can be accounted for largely by the loss of ampA mRNA in the sma knockout cells, the effect of the sma knockout on cell migration does not simply phenocopy the ampA null mutation. Cells carrying knockouts of ampA cannot migrate (Noratel et al., 2012), but sma knockouts that reduce ampA mRNA to almost undetectable levels, similar to an ampA knockout, migrate better than wild type. This indicates that Sma potentially has a role in cell migration that is independent of AmpA. By contrast, knockout of sma in the ampA overexpressing strain that reduces ampA mRNA to wild-type levels shows a severe defect in migration. Thus, in the absence of sma, ampA has an antagonistic effect on cell migration. At this point we do not have a clear idea of how AmpA influences cell migration. We know that it influences the amount of cell–substrate adhesion and that it traffics to the cell surface, is endocytosed and localizes to a perinuclear compartment that has been identified as a slow recycling compartment (Noratel et al., 2012). There is no indication that AmpA has any kind of catalytic or nucleic acid-binding role. We have suggested a possible role for ampA in recycling a cell–substrate adhesion molecule (Noratel et al., 2012). Sma clearly plays a role in reducing cell–cell adhesion and sma null cells show significantly more cell–cell adhesion than even ampA null cells, which are increased in both cell–cell and cell–substrate adhesion relative to wild type. Just how these two pathways intersect is at this point far from clear.

Sma has a role in development

An increase in Sma expression was found in developing cells, and a role during development was confirmed by the defects observed in sma^- developing cells, which failed to form fruiting bodies and arrested at mound stage. While ampA null cells delay development at mound stage, the role of Sma in development has to be larger than its role in regulating ampA mRNA levels. The ampA gene is only expressed in the Anterior-Like Cells during development whereas the sma gene is expressed in all cell types. Sma does not appear to have a role in cAMP chemotaxis during the aggregation stage of development as evidenced both from measuring its effects on chemotaxis of cells to cAMP and the fact that the sma null cells develop normally to mound stage. Could the mostly nuclear localization of Sma during migration to cAMP (early development) predict a more transcription-centered role during development while having a more cytoskeleton-actin-adhesion based role during growth?

Whatever the role of the sma gene may be, it is clearly an interesting new player in cell migration, cell adhesion and some aspects of gene expression. Dictyostelium, with its ease of molecular genetics and a full spectrum of different SAP domain-containing proteins, could prove an ideal model system in which to pursue studies of this interesting class of proteins. SAP domain-containing proteins have been shown to be involved in adenocarcinomas and leukemias emphasizing the importance of further research on this group of proteins (Choong et al., 2001; Hashii et al., 2004).

Materials and Methods

Dictyostelium growth and development

WT (AX3), ampAOE (G418 resistant), or $ampA^-$ (originally blasticidin resistant, but the blasticidin resistance cassette was removed via cre-loxP recombination (Kimmel and Faix, 2006)) cells were grown as described previously (Kelsey et al., 2012a). Low-density growing cells refers to a concentration less than 1×10^6 cells/ml. Mid-density (exponential log growth) cells were 2×10^6–5×10^6 cells/ml. High-

density cells were greater than $7{\times}10^6$ cells/ml. Cells were starved on filters to induce development (Eichinger and Rivero, 2010).

REMI mutagenesis, DNA preparation and transformations
The DNA preparation was performed as described previously (Nellen et al., 1987). Restriction enzyme mediated integration mutagenesis was from Kuspa and Shaulsky, as described by Kelsey (Kuspa, 2006; Shaulsky et al., 1996; Kelsey et al., 2012a).

Cell fractionation
Fractionation used the Thermo Scientific subcellular protein fractionation kit according to the manufacturer's instructions, as described previously (Kelsey et al., 2012a).

Sma knockout plasmid
A *sma* knockout plasmid (supplementary material Fig. S2) was constructed and used to create knockout strains in WT, *ampAOE* and *ampA⁻* backgrounds. It contained a 1 kb coding region (AB) and another 1 kb coding region (CD) downstream of the first. A 500 bp sequence was left out between the two coding regions. The AB and CD regions were inserted at *Eco*RI, *Hin*dIII and SpeI, SacII restriction sites in a pBluescript plasmid containing a floxed blasticidin resistance cassette previously inserted at a *Sma*I site (Kimmel and Faix, 2006). The fragments were inserted on either side of the cassette.

AB segment primers: forward 5′-CAGAAGCTTCAAATTTATTAGCATTA-3′, reverse 5′-CAGGAATTCAAATCTTTTTGAGCAAATTCA-3′.

CD segment primers: forward 5′-CAGACTAGTTTGCCAATGTTAAATCAA-AGG-3′, reverse 5′-CAGCCGCGGGTCGTTGTTGTTGCTGTTGG-3′.

Primers used to check for correct insertion: forward 5′-AATAGTAATGAACA-AGGTTGTG-3′, reverse 5′-TTGCATTCTATTGTACAACG-3′.

Sma-mRFP
The Sma-mRFP plasmid (supplementary material Fig. S6) was constructed to monitor Sma expression. The Sma-mRFP plasmid expresses the Sma protein region followed in frame by the mRFPmars coding sequence at the carboxy terminus of the protein (Müller-Taubenberger et al., 2006). Following the mRFPmars coding region is a 270 bp terminator sequence from the 3′ non-coding region of the *ampA* gene. A 1200 bp region of the *sma* 3′ coding sequence was inserted at ApaI and *Sal*I sites into pBluescript+Bsr, which already contained a floxed blasticidin resistant cassette previously inserted at the *Sma*I site (Kimmel and Faix, 2006). A 1500 bp region of the 3′ *sma* non-coding sequence immediately downstream of the termination site was inserted at NotI and SacII sites. *Sma* 3′ coding primers: forward 5′-GAACCTAGGGCCCTCAAGAGCAATCAGTAA-TCCA-3′, reverse 5′-GCACGCGTCGACCACAAATTATTATAGTAGAG-3′. The 3′ *sma* non-coding region primers were: forward 5′-CGCGCAATTAGCG-GCCGCCCAATACTTGAATTGGTAATA-3′, reverse 5′-ACTCGATCCGCGG-CCTCTATCTTTATTCGCTA-3′.

The Sma-mRFP plasmid was linearized by ApaI and SacII for transformation.

The primers used to check for Sma-mRFP homologous recombination into the *sma* gene were: forward 5′-CTCATTAGTAGATTCACTCTAC-3′ and reverse 5′-GCAAATCTCACTATTACCAATTC-3′.

GFP-Sma
A GFP-Sma-containing rescue plasmid (supplementary material Fig. S3) was constructed containing an N-terminal GFP coding sequence and a Gly–Pro–Gly linker sequence fused to the *sma* cDNA. The plasmid also contained an actin 15 promoter and terminator. The full length *sma* cDNA replaced the arp2/3 gene at *Bam*HI and SacI restriction sites in the GFP-Arp2/pBIG plasmid (Dicty Stock Center) (Asano et al., 2004). The primers for *sma* PCR were: forward 5′-CAGGGATCCAATGAATAAAAGAACAAGAGATAAG-3′ and reverse 5′-CAGGAGCTCTTACCACAAATTATTATAGTAGAGTG-3′.

Immunodetection
Western analysis, indirect immunofluorescence, F-actin and DAPI staining were performed as described previously (Kelsey et al., 2012a; Kelsey et al., 2012b). It was necessary to use indirect immunofluorescence microscopy with fixed cells to detect the mRFP fusion protein in *Dictyostelium* cells because the mRFP fluorescence was too weak to detect with laser power that did not kill the cells.

To calculate total cell volumes, Alexa fluor-594 conjugated deoxyribonuclease I (Molecular Probes) was added to label unpolymerized G-actin (Kelsey et al., 2012a; Kelsey et al., 2012b).

Microscopy
A Leica SP5 scanning confocal light microscope was utilized as described previously (Kelsey et al., 2012a; Kelsey et al., 2012b). Volocity software 5.5 (PerkinElmer) was used to assemble images, calculate the Pearson's coefficient of correlation (Barlow et al., 2010) and cell volume measuring the G-actin signal. Agar plates were viewed as described previously (Kelsey et al., 2012a; Kelsey et al., 2012b). Images used for calculating plaque sizes were analyzed using the Metamorph Imaging series version 7.0r1 (Universal Imaging, West Chester PA, Molecular Devices Corporation). For time-lapse experiments, cells were imaged on the Leica SP5 confocal microscope with a low laser setting (5% Argon laser line 488 nm) using brightfield illumination with either a 40× .55 NA long working objective or a 63× 1.4 NA oil objective. Z-slices of cells were captured at 20-second intervals for 5 minutes and images were processed with the Volocity or Metamorph software.

Chemotaxis
The procedure was adapted from Hadwiger and Srinivasan, and is described by Kelsey (Hadwiger and Srinivasan, 1999; Kelsey et al., 2012a). Cell movement was analyzed using DIAS (Wessels et al., 2006) and ImageJ (W.S. Rasband, ImageJ, U.S. National Institutes of Health, Bethesda, Maryland, USA, http://imagej.nih.gov/ij, 1997–2011) software. Velocity and directionality values were obtained using the manual tracking (F. Cordelieres, Manual Tracking, Institute Curie, Orsay France, http://rsb.info.nih.gov/ij/plugins/track, 2004) and chemotaxis tool (G. Trapp and E. Horn, Chemotaxis and Migration tool, Munich, Germany, http://ibidi.com) on ImageJ. The chemotactic index (CI) is equal to the cosine of the angle formed between the line of movement of the cell and the line representing direct movement to the chemoattractant (Iijima and Devreotes, 2002).

Phalloidin-binding assay to measure the amount of F-actin
As described previously (Kelsey et al., 2012b; Noratel et al., 2012).

Cell substrate adhesion assay
As described previously (Noratel et al., 2012).

RT-PCR
As described previously (Kelsey et al., 2012a; Kelsey et al., 2012b). The *ampA* primers were: 5′-TCAAATTAACACCAGTGCAAC-3′ and 5′-ATGGTTCACAACGACCACAA-3′, which yield an 870 bp product. The *sma* primers were: 5′-ATTGCATATGGCACTCAAATGA-3′ and 5′-TTACCACAAATTATTATAGTAGAGTG-3′, which yield a 1626 bp product. The control, Ig7, primers were: 5′-TTACATTTATTAGACCCGAAACCAAGCG-3′ and 5′-TTCCCTTTAGACCTATGGACCTTAGCG-3′, which yield a 370 bp fragment (Hopper et al., 1993). A gel doc digital imaging system (Alpha Innotech Corporation IS-100) was used to quantify band intensity under conditions where the signal was linearly dependent upon the amount of material loaded. Unequal protein loading or unequal RNA levels were taken into account with the Coomassie and Ig7 controls. Then the relative intensity of the bands to one another was calculated, with the most intense band set equal to 100%.

Statistical analysis
P-values were calculated using the paired two-tailed Student's *t*-test in Excel.

Competing Interests
The authors have no competing interests to declare.

References
Ahn, J. S. and Whitby, M. C. (2003). The role of the SAP motif in promoting Holliday junction binding and resolution by SpCCE1. *J. Biol. Chem.* **278**, 29121-29129.
Aravind, L. and Koonin, E. V. (2000). SAP – a putative DNA-binding motif involved in chromosomal organization. *Trends Biochem. Sci.* **25**, 112-114.
Aravind, L. and Koonin, E. V. (2001). Prokaryotic homologs of the eukaryotic DNA-end-binding protein Ku, novel domains in the Ku protein and prediction of a prokaryotic double-strand break repair system. *Genome Res.* **11**, 1365-1374.

Asano, Y., Mizuno, T., Kon, T., Nagasaki, A., Sutoh, K. and Uyeda, T. Q. (2004). Keratocyte-like locomotion in *amiB*-null *Dictyostelium* cells. *Cell Motil. Cytoskeleton* **59**, 17-27.

Bagorda, A., Mihaylov, V. A. and Parent, C. A. (2006). Chemotaxis: moving forward and holding on to the past. *Thromb. Haemost.* **95**, 12-21.

Barlow, A. L., Macleod, A., Noppen, S., Sanderson, J. and Guérin, C. J. (2010). Colocalization analysis in fluorescence micrographs: verification of a more accurate calculation of Pearson's correlation coefficient. *Microsc. Microanal.* **16**, 710-724.

Blumberg, D. D., Ho, H. N., Petty, C. L., Varney, T. R. and Gandham, S. (2002). AmpA, a modular protein containing disintegrin and ornatin domains, has multiple effects on cell adhesion and cell fate specification. *J. Muscle Res. Cell Motil.* **23**, 817-828.

Böhm, F., Kappes, F., Scholten, I., Richter, N., Matsuo, H., Knippers, R. and Waldmann, T. (2005). The SAF-box domain of chromatin protein DEK. *Nucleic Acids Res.* **33**, 1101-1110.

Casademunt, E., Varney, T. R., Dolman, J., Petty, C. and Blumberg, D. D. (2002). A gene encoding a novel anti-adhesive protein is expressed in growing cells and restricted to anterior-like cells during development of *Dictyostelium*. *Differentiation* **70**, 23-35.

Choong, M. L., Tan, L. K., Lo, S. L., Ren, E. C., Ou, K., Ong, S. E., Liang, R. C., Seow, T. K. and Chung, M. C. (2001). An integrated approach in the discovery and characterization of a novel nuclear protein over-expressed in liver and pancreatic tumors. *FEBS Lett.* **496**, 109-116.

Devreotes, P. and Janetopoulos, C. (2003). Eukaryotic chemotaxis: distinctions between directional sensing and polarization. *J. Biol. Chem.* **278**, 20445-20448.

Du, K. L., Chen, M., Li, J., Lepore, J. J., Mericko, P. and Parmacek, M. S. (2004). Megakaryoblastic leukemia factor-1 transduces cytoskeletal signals and induces smooth muscle cell differentiation from undifferentiated embryonic stem cells. *J. Biol. Chem.* **279**, 17578-17586.

Eichinger, L. and Rivero, F. (2010). *Dictyostelium Discoideum Protocols*. Totowa, NJ: Humana Press.

Gaudet, P., Williams, J. G., Fey, P. and Chisholm, R. L. (2008). An anatomy ontology to represent biological knowledge in *Dictyostelium discoideum*. *BMC Genomics* **9**, 130.

Gaudet, P., Fey, P., Basu, S., Bushmanova, Y. A., Dodson, R., Sheppard, K. A., Just, E. M., Kibbe, W. A. and Chisholm, R. L. (2011). dictyBase update 2011: web 2.0 functionality and the initial steps towards a genome portal for the Amoebozoa. *Nucleic Acids Res.* **39 Suppl. 1**, D620-D624.

Hadwiger, J. A. and Srinivasan, J. (1999). Folic acid stimulation of the Gα4 G protein-mediated signal transduction pathway inhibits anterior prestalk cell development in *Dictyostelium*. *Differentiation* **64**, 195-204.

Hashii, Y., Kim, J. Y., Sawada, A., Tokimasa, S., Hiroyuki, F., Ohta, H., Makiko, K., Takihara, Y., Ozono, K. and Hara, J. (2004). A novel partner gene CIP29 containing a SAP domain with MLL identified in infantile myelomonocytic leukemia. *Leukemia* **18**, 1546-1548.

Hopper, N. A., Harwood, A. J., Bouzid, S., Véron, M. and Williams, J. G. (1993). Activation of the prespore and spore cell pathway of Dictyostelium differentiation by cAMP-dependent protein kinase and evidence for its upstream regulation by ammonia. *EMBO J.* **12**, 2459-2466.

Iijima, M. and Devreotes, P. (2002). Tumor suppressor PTEN mediates sensing of chemoattractant gradients. *Cell* **109**, 599-610.

Janetopoulos, C. and Firtel, R. A. (2008). Directional sensing during chemotaxis. *FEBS Lett.* **582**, 2075-2085.

Kelsey, J. S., Fastman, N. M. and Blumberg, D. D. (2012a). Evidence of an evolutionarily conserved LMBR1 domain-containing protein that associates with endocytic cups and plays a role in cell migration in *Dictyostelium discoideum*. *Eukaryot. Cell* **11**, 401-416.

Kelsey, J. S., Fastman, N. M., Noratel, E. F. and Blumberg, D. D. (2012b). Ndm, a coiled-coil domain protein that suppresses macropinocytosis and has effects on cell migration. *Mol. Biol. Cell* **23**, 3407-3419.

Kimmel, A. R. and Faix, J. (2006). Generation of multiple knockout mutants using the Cre-*loxP* system. *Methods Mol. Biol.* **346**, 187-199.

Kipp, M., Göhring, F., Ostendorp, T., van Drunen, C. M., van Driel, R., Przybylski, M. and Fackelmayer, F. O. (2000). SAF-Box, a conserved protein domain that specifically recognizes scaffold attachment region DNA. *Mol. Cell. Biol.* **20**, 7480-7489.

Kortholt, A., Kataria, R., Keizer-Gunnink, I., Van Egmond, W. N., Khanna, A. and Van Haastert, P. J. (2011). *Dictyostelium* chemotaxis: essential Ras activation and accessory signalling pathways for amplification. *EMBO Rep.* **12**, 1273-1279.

Kuspa, A. (2006). Restriction enzyme-mediated integration (REMI) mutagenesis. *Methods Mol. Biol.* **346**, 201-209.

Leslie, N. R., Yang, X., Downes, C. P. and Weijer, C. J. (2005). The regulation of cell migration by PTEN. *Biochem. Soc. Trans.* **33**, 1507-1508.

Miralles, F., Posern, G., Zaromytidou, A. I. and Treisman, R. (2003). Actin dynamics control SRF activity by regulation of its coactivator MAL. *Cell* **113**, 329-342.

Müller-Taubenberger, A., Vos, M. J., Böttger, A., Lasi, M., Lai, F. P., Fischer, M. and Rottner, K. (2006). Monomeric red fluorescent protein variants used for imaging studies in different species. *Eur. J. Cell Biol.* **85**, 1119-1129.

Nellen, W., Datta, S., Reymond, C., Sivertsen, A., Mann, S., Crowley, T. and Firtel, R. A. (1987). Molecular biology in Dictyostelium: tools and applications. *Methods Cell Biol.* **28**, 67-100.

Noratel, E. F., Petty, C. L., Kelsey, J. S., Cost, H. H., Basappa, N. and Blumberg, D. D. (2012). The adhesion modulation protein, AmpA localizes to an endocytic compartment and influences substrate adhesion, actin polymerization and endocytosis in vegetative Dictyostelium cells. *BMC Cell Biol.* **13**, 29.

Pagni, M., Ioannidis, V., Cerutti, L., Zahn-Zabal, M., Jongeneel, C. V., Hau, J., Martin, O., Kuznetsov, D. and Falquet, L. (2007). MyHits: improvements to an interactive resource for analyzing protein sequences. *Nucleic Acids Res.* **35 Suppl. 2**, W433-W437.

Parent, C. A. (2004). Making all the right moves: chemotaxis in neutrophils and *Dictyostelium*. *Curr. Opin. Cell Biol.* **16**, 4-13.

Parent, C. A. and Devreotes, P. N. (1999). A cell's sense of direction. *Science* **284**, 765-770.

Parent, C. A., Blacklock, B. J., Froehlich, W. M., Murphy, D. B. and Devreotes, P. N. (1998). G protein signaling events are activated at the leading edge of chemotactic cells. *Cell* **95**, 81-91.

Rivero, F. and Somesh, B. P. (2002). Signal transduction pathways regulated by Rho GTPases in *Dictyostelium*. *J. Muscle Res. Cell Motil.* **23**, 737-749.

Rivero, F., Muramoto, T., Meyer, A. K., Urushihara, H., Uyeda, T. Q. and Kitayama, C. (2005). A comparative sequence analysis reveals a common GBD/FH3-FH1-FH2-DAD architecture in formins from *Dictyostelium*, fungi and metazoa. *BMC Genomics* **6**, 28.

Shaulsky, G., Escalante, R. and Loomis, W. F. (1996). Developmental signal transduction pathways uncovered by genetic suppressors. *Proc. Natl. Acad. Sci. USA* **93**, 15260-15265.

Varney, T. R., Casademunt, E., Ho, H. N., Petty, C., Dolman, J. and Blumberg, D. D. (2002a). A novel *Dictyostelium* gene encoding multiple repeats of adhesion inhibitor-like domains has effects on cell–cell and cell–substrate adhesion. *Dev. Biol.* **243**, 226-248.

Varney, T. R., Ho, H., Petty, C. and Blumberg, D. D. (2002b). A novel disintegrin domain protein affects early cell type specification and pattern formation in *Dictyostelium*. *Development* **129**, 2381-2389.

Wessels, D., Kuhl, S. and Soll, D. R. (2006). Application of 2D and 3D DIAS to motion analysis of live cells in transmission and confocal microscopy imaging. *Methods Mol. Biol.* **346**, 261-279.

Witke, W., Schleicher, M. and Noegel, A. A. (1992). Redundancy in the microfilament system: abnormal development of Dictyostelium cells lacking two F-actin cross-linking proteins. *Cell* **68**, 53-62.